

AD-A189 447

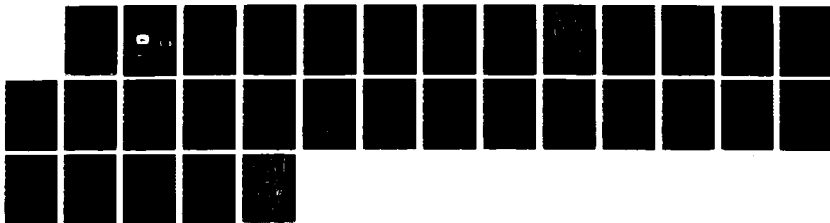
PASSIVE DF A TUTORIAL PART 1(U) JET PROPULSION LAB
PASADENA CA ALGORITHM ANALYSIS SUBGROUP 8 BUCKLES
30 APR 87 JPL-D-4825 NAS7-918

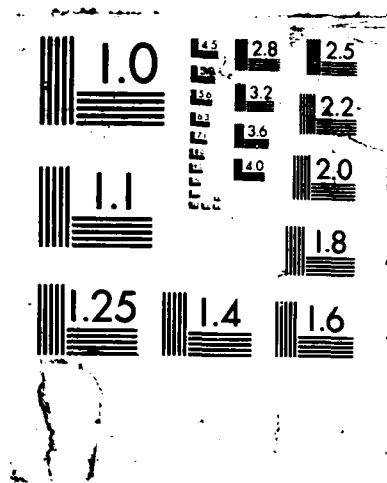
171

UNCLASSIFIED

F/G 17/11

NL





2

7057-73

DTIC FILE COPY

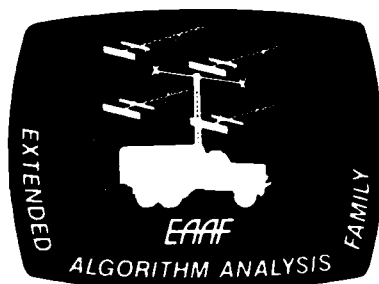
**U.S. ARMY INTELLIGENCE CENTER AND SCHOOL
SOFTWARE ANALYSIS AND MANAGEMENT SYSTEM**

**PASSIVE DF: A TUTORIAL
PART I**

TECHNICAL MEMORANDUM No. 28

Bill Buckles

AD-A189 447



DTIC
ELECTE
DEC 30 1987
S H D

30 April 1987

National Aeronautics and
Space Administration

JPL

JET PROPULSION LABORATORY
California Institute of Technology
Pasadena, California

JPL D-4625
ALGO_PUB_0098

DISTRIBUTION STATEMENT A

Approved for public release;
Distribution Unlimited

REPORT DOCUMENTATION PAGE		READ INSTRUCTIONS BEFORE COMPLETING FORM
1. REPORT NUMBER ALGO-PUB-0098	2. GOVT ACCESSION NO. AD-A189447	3. RECIPIENT'S CATALOG NUMBER
4. TITLE (and Subtitle) Technical Memo 28, "Passive DF, A Tutorial, Part I"		5. TYPE OF REPORT & PERIOD COVERED FINAL
7. AUTHOR(s) B. Buckles		6. PERFORMING ORG. REPORT NUMBER D-4625
9. PERFORMING ORGANIZATION NAME AND ADDRESS Jet Propulsion Laboratory ATTN: 171-209 California Institute of Technology 4800 Oak Grove, Pasadena, CA 91109		8. CONTRACT OR GRANT NUMBER(s) NAS7-918
11. CONTROLLING OFFICE NAME AND ADDRESS Commander, USAICS ATTN: ATSI-CD-SF Ft. Huachuca, AZ 85613-7000		10. PROGRAM ELEMENT, PROJECT, TASK AREA & WORK UNIT NUMBERS RE 182 AMEND #187
14. MONITORING AGENCY NAME & ADDRESS (if different from Controlling Office) Jet Propulsion Laboratory, ATTN: 171-209 California Institute of Technology 4800 Oak Grove, Pasadena, CA 91109		12. REPORT DATE 30 Apr 87
		13. NUMBER OF PAGES 25
		15. SECURITY CLASS. (of this report) UNCLASSIFIED
		15a. DECLASSIFICATION/DOWNGRADING SCHEDULE NONE
16. DISTRIBUTION STATEMENT (of this Report) Approved for Public Dissemination		
17. DISTRIBUTION STATEMENT (of the abstract entered in Block 20, if different from Report) Prepared by Jet Propulsion Laboratory for the US Army Intelligence Center and School's Combat Developer's Support Facility.		
18. SUPPLEMENTARY NOTES		
19. KEY WORDS (Continue on reverse side if necessary and identify by block number) Passive Intercept, Direction of Arrival, Amplitude Comparison, Phase Interferometry, Multiple Baseline, DF Accuracy		
20. ABSTRACT (Continue on reverse side if necessary and identify by block number) This memo introduces passive intercept and emitter identification problems. Then precision Direction of Arrival (DOA) methods and algorithms are introduced. The algorithms for amplitude comparison and phase interferometry are discussed in detail. four other types of location algorithms are also examined. The memo concludes with a cross-comparison of these methods.		

7057-73

U.S. ARMY INTELLIGENCE CENTER AND SCHOOL
Software Analysis and Management System

Passive DF: A Tutorial
Part I

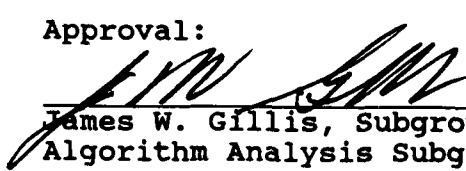
Technical Memorandum No. 28

30 April 1987

Author:

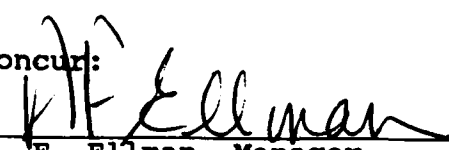

Bill Buckles, Consultant

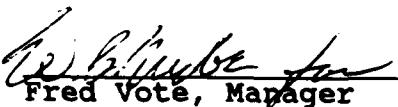
Approval:


James W. Gillis, Subgroup Leader
Algorithm Analysis Subgroup


Edward J. Records, Supervisor
USAMS Task

Concur:


A. F. Ellman, Manager
Ground Data Systems Section


Fred Vote, Manager
Advanced Tactical Systems

JET PROPULSION LABORATORY
California Institute of Technology
Pasadena, California

JPL D-4625



Accession For	
NTIS GRA&I	<input checked="" type="checkbox"/>
DTIC TAB	<input type="checkbox"/>
Unannounced	<input type="checkbox"/>
Justification	
By	
Distribution/	
Availability Codes	
Dist	Avail and/or Special
A-1	

PREFACE

The work described in this publication was performed by the Jet Propulsion Laboratory, an operating division of the California Institute of Technology, under contract NAS7-918, RE182, A187 with the National Aeronautics and Space Administration, for the United States Army Intelligence Center and School.

This specific work was performed in accordance with the FY-87 statement of work (SOW #2).

EXECUTIVE SUMMARY

This Technical Memorandum was prepared originally as part of the Generic Fix Report (FY-86) which was eliminated under the FY-87 statement of work (SOW #2), undated (delivered to JPL 19 November 1986).

The purpose of the Generic Fix Report, of which this paper was to be an appendix, was to collect all the material needed to understand Direction Finding and Fix Estimation and their mathematical basis in one volume to support the multi-volume series of Fix Estimation Reports.

This paper is being published because of its tutorial value. It will be of value to readers desiring to more fully understand the DF process underlying the Fix Estimation Reports.

PASSIVE DF: A TUTORIAL

PART I

PREPARED BY
BILL BUCKLES

Section I. Introduction

Why Passive Intercept

Intercept systems provide critically important data that can influence the outcome of a military engagement, as was illustrated by the actions in Lebanon and the Falkland Islands. Israeli success in eliminating the Syrian surface-to-air missile sites was due, in part, to information gathered by ELINT systems. Similarly, the success of the EXOCET missile in destroying the British ship HMS Sheffield emphasizes the need for early warning, identification, and location of radiating hostile forces.

Passive intercept systems provide emitter ID and location. This information can give insight into hostile weapon systems type and the immediacy of any possible threat, as well as target coordinates that would allow neutralization of the threat. This information is used during peace time to keep track of the deployment of potentially hostile military weapon systems. During wartime, it is used for prestrike planning and for assessing poststrike damage. Because these systems work in a passive mode, they perform their task without revealing their position or even their presence to the enemy.

Emitter Identification

Emitter identification requires the isolation of intercepted signals. Signal isolation is the process of identifying and associating consecutive pulses produced by the same emitter from a population of pulses that occur simultaneously in the receiver i.f. passband. Radar parameters that are measured on each pulse (e.g., frequency, pulsewidth, pulse amplitude, and direction of arrival) may be used in the signal isolation process. In some cases, due to the density of the signal environment, a pulse train deinterleaving process which further sorts emitters based upon their pulse interval pattern is also used. Most modern Electronic Support Measures (ESM) systems perform a monopulse sorting function, then verify that the sorted pulses are from a single emitter, through various deinterleaving routines. These routines range from simple pulse interval prediction to autocorrelation techniques which are required to recognize some of the more modern agile pulse repetition interval (PRI) radars.

Once a signal is isolated, the single pulse parameters are combined with the derived pulse repetition pattern and the emitter's scan rate (which

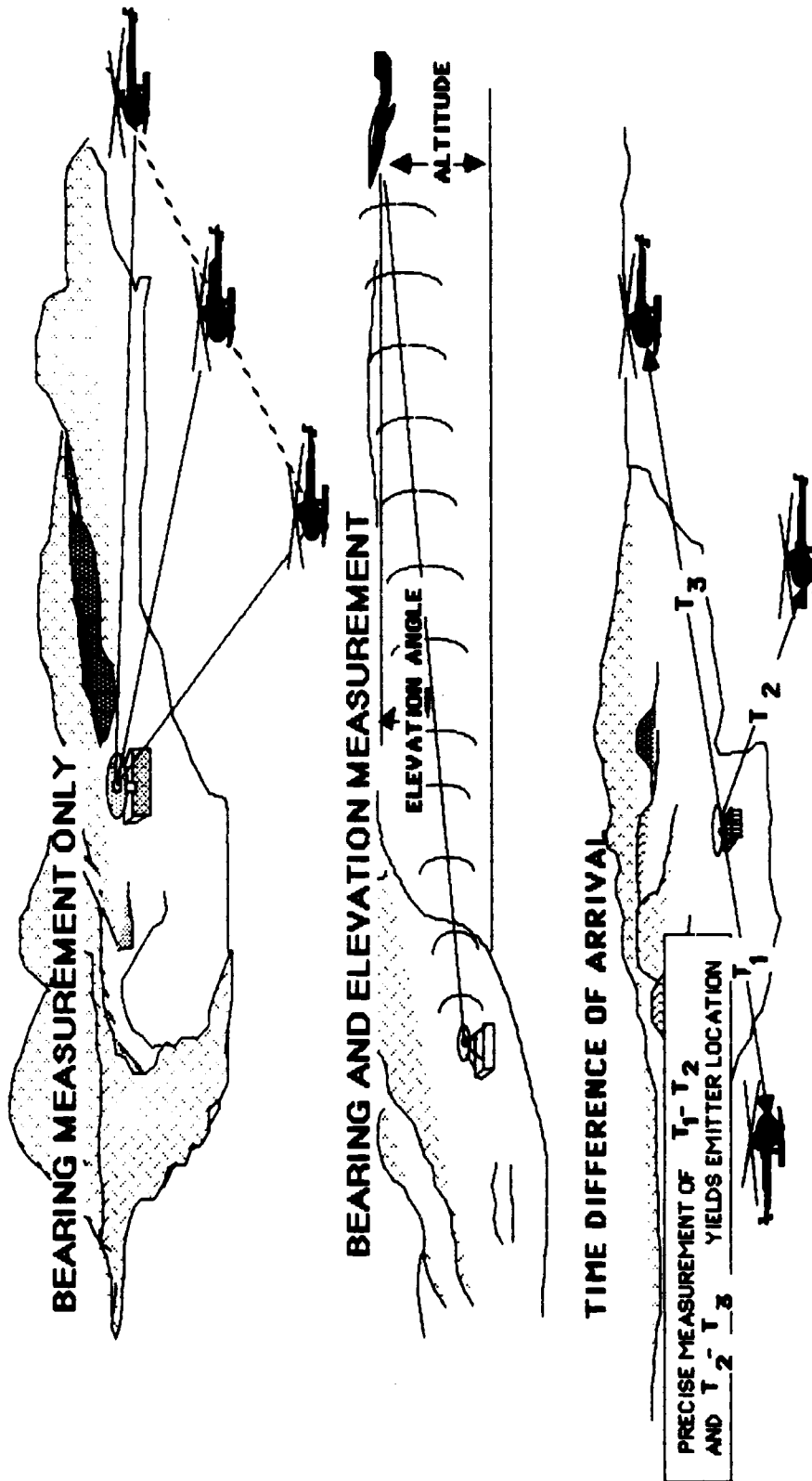


FIGURE 1. PASSIVE LOCATION

is derived by processing the pulse amplitude measurements) to identify the emitter. This is done by matching measured parameters with a previously stored parameter listing.

Precision DOA

Accurate measurement of the signal's direction of arrival is vital in performing both the emitter identification and location functions. The signal isolation process has become more difficult due to increased radar parameter (frequency, PRI) agility and to increased numbers of signals in the passband due to higher emitter densities and the use of wider bandwidth receivers. Since the emitter's direction of arrival is not easily varied, it provides a very reliable monopulse sorting parameter.

Highly directional jamming antennas are used to increase jamming power, so as to more effectively screen penetrating aircraft. Aircraft motion and rapid maneuvering require precise real time measurement of the victim radar's azimuth and elevation angle. These measurements are used to point the jamming antennas in azimuth and elevation. This passive angular steering function is also being extended to other narrow field of view systems, such as infrared missile seekers, laser range finders, and TV. While these sensors provide excellent angular resolution and accuracy, they have very narrow fields of view, requiring a time consuming search that greatly decreases the probability of interception. This

may be eliminated, if the target is radiating, by the use of a passive direction finding system, which has an inherently wide field of view. For example, two orthogonal arrays could measure an emitter's azimuth and elevation angles with high accuracy and resolution. This angular data could then be used to set the narrow beamwidth optical sensor on target, thereby creating a much more efficient system.

Passive Techniques

Accurate, timely determination of emitter location is vital to all phases of military activity. The detection of significant movement of weapon associated radars could be a precursor to hostile actions. During hostilities, knowing the location of a hostile fire control radar would allow neutralization prior to other offensive actions. Very precise emitter location enables strike aircraft to use conventional weapons and bombs by geographical coordinates. Knowledge of emitter range permits threat prioritization and effective allocation of weapons and jammers. Almost all conceivable properties and characteristics of RF signals have been used in an attempt to passively derive emitter location. This paper addresses passive location of ground emitters. The emitter location techniques reviewed are depicted in Figure 1. Both conventional triangulation via DOA measurements and the phase rate of change extension of this technique are considered. The phase rate of change technique derives location much faster than the conventional triangulation

method and requires fewer antenna/receiver channels.

The azimuth/elevation (AZ/EL) location technique is also reviewed. It yields single pulse instantaneous measurement of emitter location and is very effective if the altitude of both the emitter and measurement platform are known, and if the depression angle is large.

Finally, The multiple aircraft time difference of arrival (TDOA) technique is reviewed. This is an extension of phase interferometry, except that the distance between antenna elements is measured in miles and not inches; and therefore, very measurable time differences are produced. Not only must the time difference of arrival measurement be made very precisely, but the specific location of each aircraft must be accurately known. Other location techniques that have been used include the comparison of received signal power with estimates of effective radiated power (ERP), and measurement of the time difference of arrival between the direct and reflected paths. These techniques will not be addressed here because they have not been found consistently reliable since they are very sensitive to propagation anomalies.

SECTION II. DF TECHNIQUES

Amplitude Comparison

The comparison of received signal amplitude between antennas is one of the most often used direction finding techniques. Amplitude comparison DF is used by almost all of the radar warning receiving (RWRs) systems that have been deployed. The typical system consists of four broad bandwidth, orthogonally oriented antennas which provide 360° of coverage around the platform. The technique determines gross direction of arrival on the basis of which antenna has the strongest received signal. A comparison of amplitudes between adjacent antennas yields a fine DF measurement. If each antenna has its own dedicated receiver, these measurements can be performed simultaneously, thus providing a monopulse DF capability. Accuracies of 3° to 10° can be achieved with such systems. Figure 2 depicts the basic amplitude comparison technique. Antennas 1 and 2 are separated by the squint angle, S, where $S = \theta_1 + \theta_2$. The direction of arrival of the signal is at an angle, B, from the array boresight of the two antennas. The amplitude comparison measurement is based on the ratio, C, of the signal level received by antenna 2 relative to the signal received by antenna 1. By using the known shape of the antenna patterns as a function of azimuth, the DOA of the signal may be determined. A typical RWR system utilizing four antennas squinted at 90° to provide 360° of coverage

is illustrated in Figure 3. For broad bandwidth antennas with Gaussian shaped gain patterns, it can be shown that the measured DF angle is given by:

$$B = \frac{\theta_{BW}^2 C}{48.1 (S/2)} \quad (1)$$

where

- θ_{BW} = Beamwidth of the Antennas in Degrees
- C = Amplitude Comparison Ratio in db
- S = Squint Angle in Degrees

The DF accuracy (ΔB) is thus a direct function of the amplitude tracking between antenna channels. The expression for DF accuracy is given by the following equation.

$$\Delta B = \frac{\theta_{BW}^2 \Delta C}{48.1 (S/2)} \quad (2)$$

Note that as the true DOA shifts away from the antenna patterns crossover point the gain in one channel decreases. This results in a decrease in signal-to-noise ratio (SNR). For signals near the receiver threshold this could result in a large measurement error. Therefore, for signals near threshold, DF accuracy and resolution degrade as the AOA

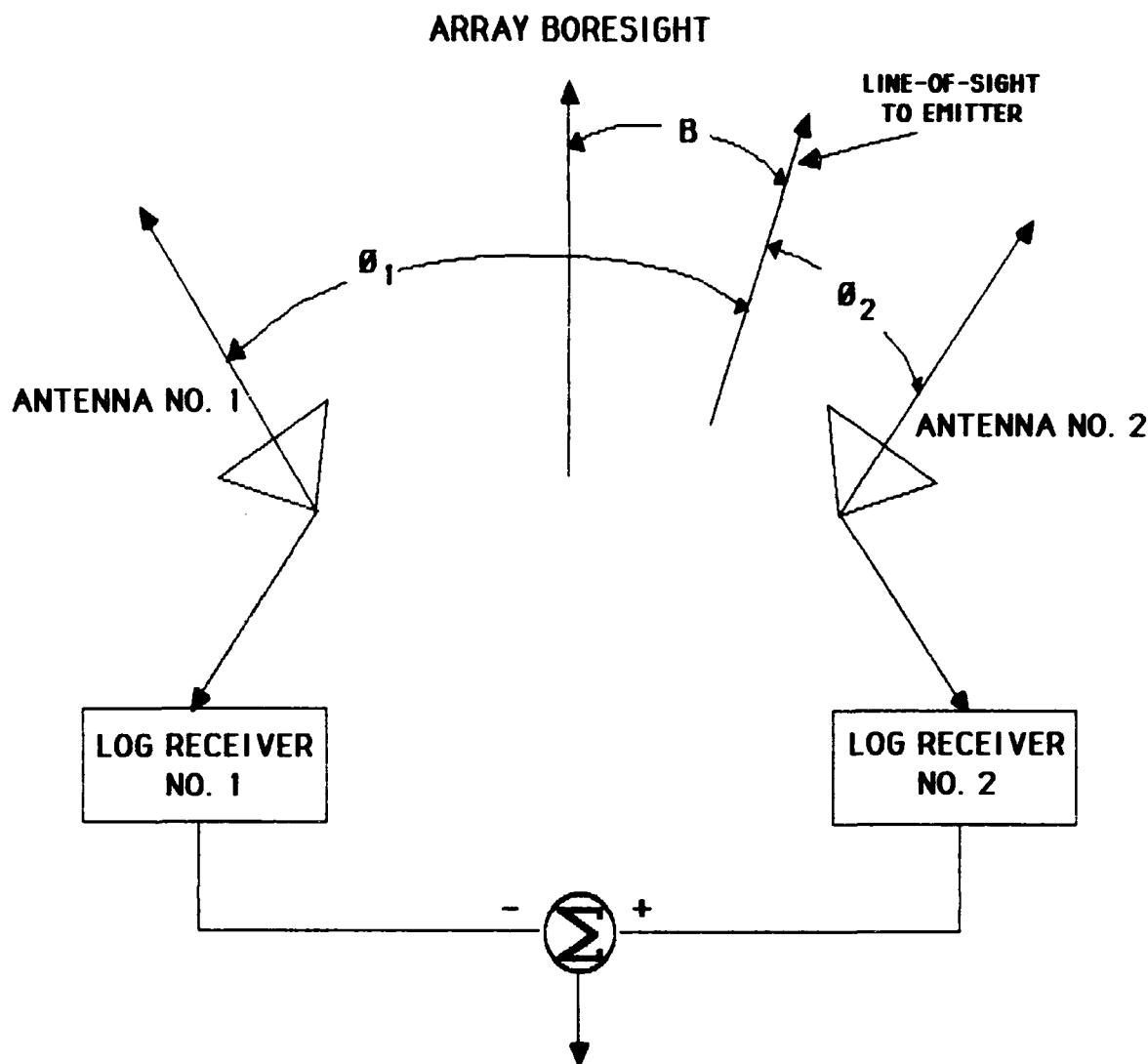


FIGURE 2. AMPLITUDE COMPARISON DF TECHNIQUE

moves away from the pattern crossover. If $S = 0$, then, from equation 2, the amplitude mistrack equation reduces to equation 3

$$\Delta B = \frac{\phi_{BW} \Delta C}{24.05} \quad (3)$$

For this condition, adding more antennas with reduced beamwidths provides higher DF accuracy and sen-

sitivity; this results, however, in the need for additional receiver channels and, of course, increases the weight and volume requirements of the system. The amplitude mistrack between any two channels is a function of how closely the various components of the system are matched, as well as the SNR at which the comparison is made. Calibration techniques are often employed to reduce the amplitude

mistrack due to these variations. Averaging pulse amplitude measurements can also be used to reduce mistrack error. For an octave bandwidth system amplitude mistrack due to component variation tends to be about 3 db and may be reduced to about 1 db by careful calibration. For signals near threshold, noise can contribute another 1.4 db of mistrack (this can be reduced to .5 db if multi-pulse averaging is used). The amplitude mistrack is the Root-Sum-Square (RSS) of the component and noise induced mistrack errors. The single channel amplitude error due to receiver noise is:

$$\Delta A = \frac{6.14 \text{ db}}{\text{SNR}} \quad (4)$$

For a threshold signal, the total mistrack is 3.3 db (component mistrack of 3 db and 1.4 db amplitude mistrack resulting from a SNR of 16 db). If a calibration reduces component mistrack to 1 db from 3 db then the total mistrack becomes 1.7 db. This can be further reduced to 1.1 db if eight pulses are averaged. Table 1 shows how the DOA accuracy varies with antenna beamwidth and the number of antennas for amplitude mistrack of 3.3, 1.7, and 1.1 db. The DF accuracy will be best where the slopes of the antenna patterns are greatest. Thus, adding antennas with the same beamwidth and reducing the squint angle degrades the DOA accuracy but does improve the system sensitivity at crossover. Alternatively, reducing

the beamwidth while maintaining the squint angle improves the DOA accuracy but at the expense of sensitivity at the antenna pattern crossover points. Reducing the beamwidth and squint together allows an improvement in accuracy without reducing sensitivity, but requires additional antennas to retain 360° azimuthal coverage. Figure 4 presents the allowable RMS amplitude mistrack vs. antenna beamwidth, and number of antennas required to provide 360° coverage for various DOA accuracies. The squint angle in this case is taken to be equal to the beamwidth of the antenna. As can be seen, a four antenna 360° system with a total 3 db mistrack will have a DF accuracy of approximately 12°, which may be reduced by calibration to about 4°. To achieve a 1° system, both calibration and the use of as many as 16 antennas would be required. Amplitude comparison DF systems have most often been deployed with broadband crystal video receivers in radar warning systems. This approach, however, is equally applicable to superheterodyne receivers and is being applied to acoustic/optical receivers.

PHASE INTERFEROMETRY **SINGLE BASELINE THEORY**

The phase interferometer concept is shown in Figure 5. A pair of wide beamwidth antennas are separated by a distance, d . The plane wave arriving at an angle is received by one antenna earlier than the other, due to the difference in path length, a . This path length difference.

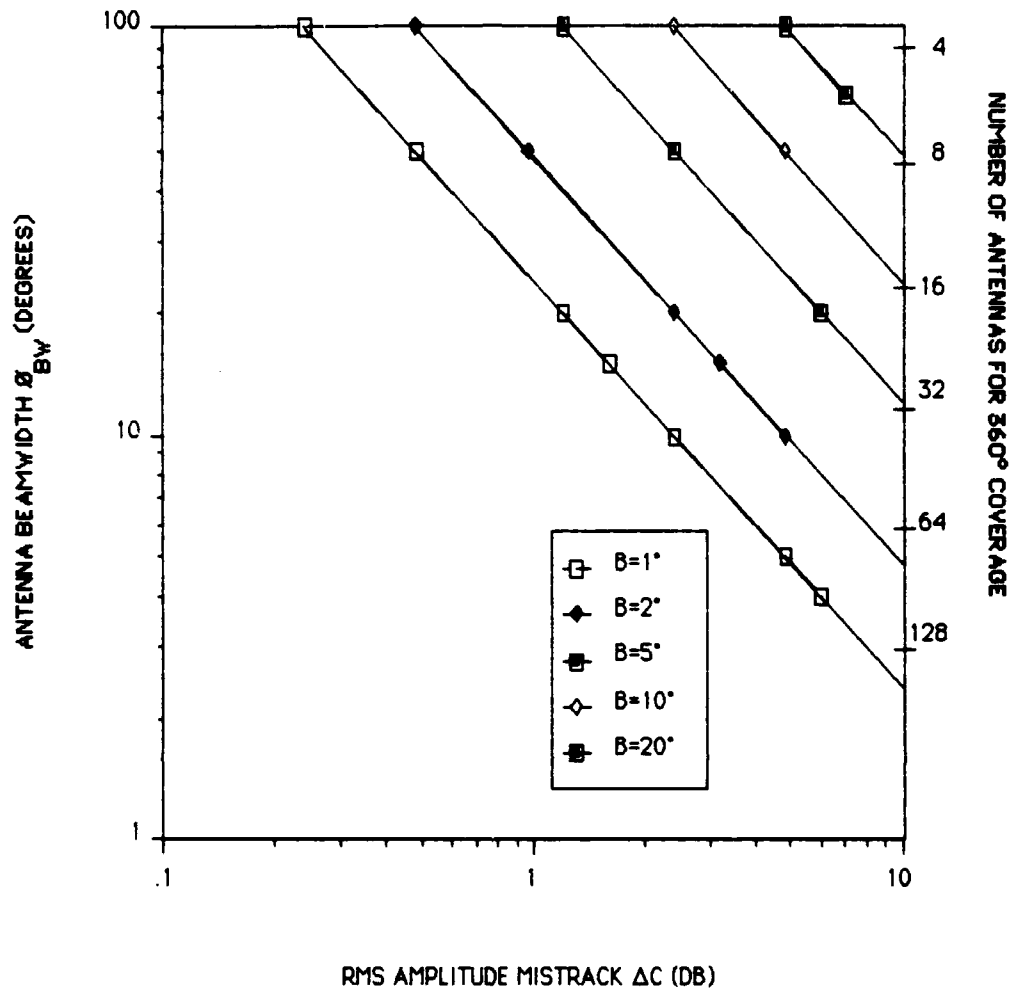
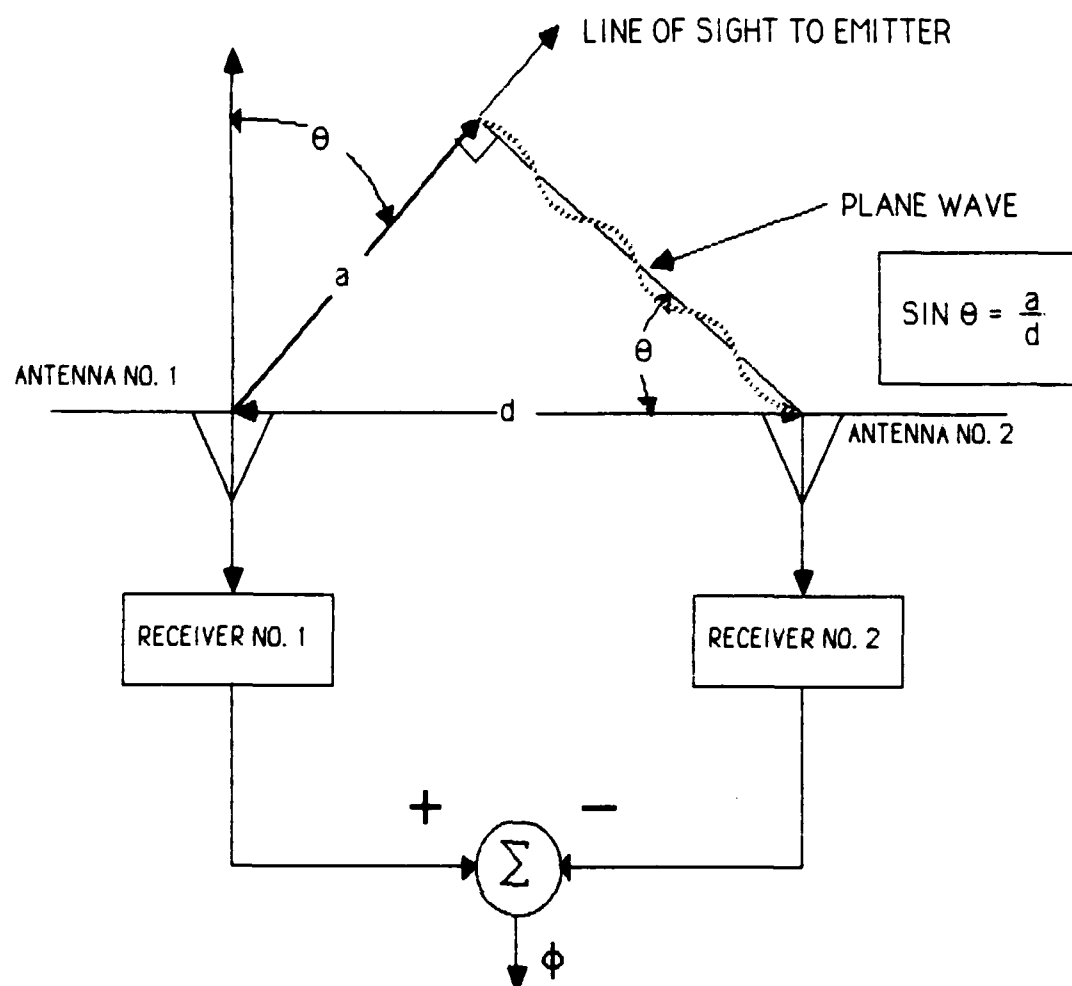


FIGURE 4. AMPLITUDE MISTRACK AND BEAMWIDTH REQUIREMENTS FOR VARIOUS DOA ACCURACIES

NUMBER OF ANTENNAS	SQUINT ANGLE θ (DEGREES)	ANTENNA BEAMWIDTH θ_{BW} (DEGREES)	DOA ACCURACY SENSITIVITY ($\Delta\theta/\Delta C$) (DEGREES/DB)	DOA ACCURACY IN DEGREES			SENSITIVITY DEGRADATION (DB)
				SINGLE PULSE NOT CALIBRATED $\Delta C=3.3$ DB	SINGLE PULSE CALIBRATED $\Delta C=1.7$ DB	8 PULSE AVG CALIBRATED $\Delta C=1.1$ DB	
4	90	70	2.26	7.5	3.8	2.5	4.98
		90	3.74	12.3	6.4	4.1	3.00
8	45	45	1.88	6.2	3.2	2.1	3.00
		70	4.53	14.9	7.7	5.0	1.24
		90	7.48	24.7	12.7	8.2	0.75
8	135	70	1.51	5.0	2.6	1.7	11.2
		90	2.49	8.2	4.2	2.7	6.77

TABLE 1. DOA ACCURACY AND SENSITIVITY OF TYPICAL AMPLITUDE COMPARISON SYSTEMS FOR AN EMITTER AT THE ARRAY BORESIGHT



$$\begin{aligned} \phi &= \frac{a}{\lambda} \text{ cycles } 360^\circ/\text{cycle} = \frac{360 a}{\lambda} \\ &= \frac{360 d}{\lambda} \sin \theta \\ \text{SPATIAL ACCURACY } \Delta \theta &= \frac{\Delta \phi}{\frac{360 d}{\lambda}} \quad \cos \theta = \frac{\Delta \phi c}{360 d f \cos \theta} \\ \text{UNAMBIGUOUS FIELD OF VIEW } \theta_{\text{UNAMBIGUOUS}} &= 2 \sin^{-1}(\lambda/2 d) \end{aligned}$$

FIGURE 5. BASIC PHASE INTERFEROMETER

manifests itself both as a difference in the time of arrival of the signal at each antenna and as a phase difference, ϕ , between the RF signals at each antenna. Equation 5 is the expression for this phase difference.

$$\phi = \frac{360 \, d \sin \theta}{\lambda} \quad (5)$$

Because typically $d = 1$ to 2 feet for airborne interferometers, the actual time difference is usually less than 1 nanosecond. Direct measurement would require a wide bandwidth receiver, a precise clock, and high speed logic. The wide bandwidth degrades system sensitivity and also increases the number of signals that must be sorted. Consequently, the time difference of arrival technique is only used when the antennas can be placed on separate platforms which are separated by several miles, as described later in this tutorial. Since the phase difference between the signals at each antenna is preserved for the duration of the pulse, this parameter can be easily measured. The video bandwidth need only be compatible with the minimum pulse to be measured. For a 100 nanosecond pulse, the bandwidth could be as small as 5 MHz, which is consistent with the sensitivities and selectivities of modern ESM systems. The interferometer antennas have wide beamwidths (typically 90°). DF accuracy and resolution are achieved by receiver processor techniques. While this is an advantage in that high probability of intercept is

provided, it is also a disadvantage in that time coincident pulsed signals coming from different angles of arrival and falling within the IF pass-band will interfere with each other. If they are relatively close in amplitude, large errors in the direction of arrival measurement will result. Most of the time simultaneous signals will separate in time, permitting precise DF measurement of both signals.

The interferometer measures the incident angle between the two antennas and not the azimuth angle. The relationship between the incident angle, the azimuth angle, and the elevation angle is shown in Figure 6. The locus of points which produce the same incident angle as a function of the azimuth and elevation angle form a cone. An error will be made if the incident angle is assumed to be the same as the azimuth angle. The error is negligible for signals arriving near zenith and elevation angle boresight. At 45° and 10° elevation angles, the error increases significantly with elevation angle. Thus, if both the azimuth and elevation angles are 45° , the error is 15° . This error results even if there are no instrumentation errors. This error can be eliminated if two interferometer arrays are used to measure the angles of arrival. For example, two orthogonal arrays could simultaneously measure the azimuth and elevation angles. Note that two horizontal interferometer elements with overlapping fields of view can also yield the azimuth and elevation angles, and, in fact, any two linearly

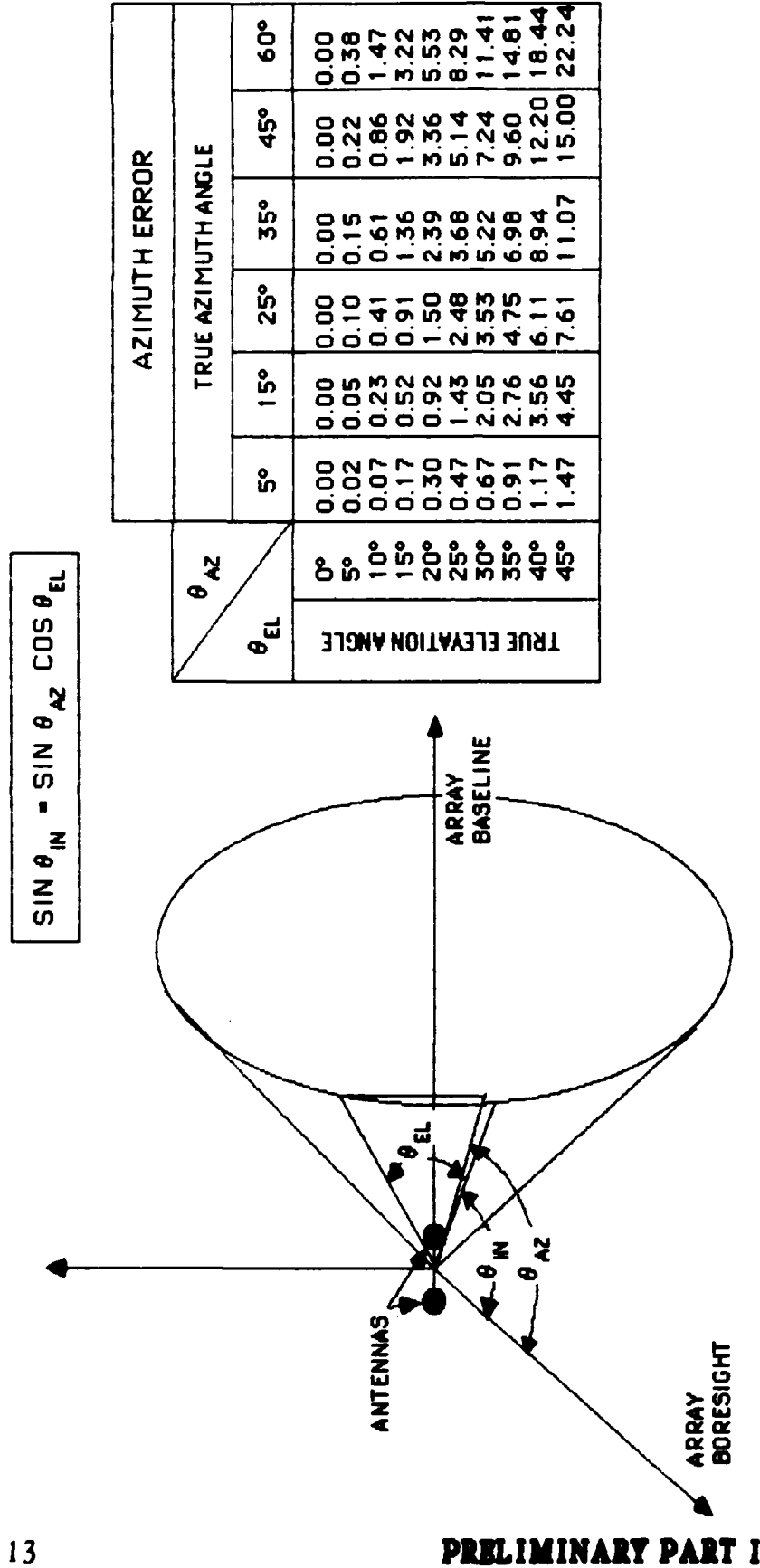


FIGURE 6. WHY THE INCIDENT ANGLE IS NOT THE SAME AS THE AZIMUTH ANGLE

independent measurements are sufficient since there are only two unknowns to be derived. For some military applications, which are primarily interested in targets near the horizon, the depression angle is small and only horizontal arrays are used. The unambiguous field of view, θ_u , of the two element interferometer is given by equation 6

$$\theta_u = 2 \sin^{-1} (\lambda/2d) \quad (6)$$

This is obtained by solving equation 5 for θ and recognizing that ϕ is uniquely related to θ over the range of $\phi = \pm 180^\circ$. Since $\sin \theta$ has maximum values of ± 1 , for the unambiguous field of view to be $\pm 90^\circ$, d must be less than $\lambda/2$. If d is greater than $\lambda/2$ the unambiguous angle is less than $\pm 90^\circ$. In other words, different spacial angles of arrivals in the same hemisphere will yield the same phase.

The spatial angular error, $\Delta\theta$, as a function of the electrical phase error, $\Delta\phi$, is readily derived by differentiating equation 5 to obtain.

$$\begin{aligned} \Delta\theta &= \frac{\Delta\phi}{(360d/\lambda)(\cos\theta)} \\ &= \frac{\Delta\phi c}{(360df\cos\theta)} \end{aligned} \quad (7)$$

where

$\Delta\theta$ = spatial angular error
 $\Delta\phi$ = electrical phase error
 θ = spatial angle of arrival
 d = end element spacing
 f = frequency
 c = speed of light

The spatial angular error for a given phase error is reduced as d gets larger. This then is the attractiveness of interferometers. By increasing the baseline one can reduce the DOA error to an arbitrarily small value in spite of large phase errors. Of course, increasing d beyond $\lambda/2$ for the simple two element interferometer reduces the unambiguous field of view. The challenge of multibaseline interferometer design is to obtain precision DOA unambiguously over the required field of view and over broad bandwidths, while using a minimum number of antenna/receiver channels that do not require ultra precise component phase tracking or elaborate calibration routines. It should also be noted from equation 7 that the spatial angular error increases as $1/\cos\theta$, as the angle of arrival, θ , varies from boresight. Thus at 45° , the error is approximately 40% larger than it is at boresight. At 90° off boresight, the error would become infinite, but, in fact, most systems use quadrant arrays so that the adjacent quadrant array provides boresight accuracy. It is also seen that, for a given interferometer spacing, the spatial angular error increases as the frequency is reduced.

PHASE INTERFEROMETRY MULTIPLE BASELINE THEORY

The multiple baseline interferometer, which combines high ac-

curacy with a wide unambiguous field of view, is conceptually illustrated in Figure 7. A plane wave impinges upon the array of nondirectional antennas. As the baseline increases, the phase difference increases with respect to the reference antenna. The phase difference is measured by a phase discriminator in the receiving system. The phase discriminator produces two outputs: $\sin\phi$ and $\cos\phi$. Techniques have been developed that quantize the phase unambiguously over ± 180 electrical degrees by processing these outputs. Very rapid response time is obtained since these techniques do not require sample and hold circuitry. Quantization from 2 to 8 bits has been achieved.

For the purpose of illustration Figure 7 depicts 4-bit phase quantization. The cells are plotted in electrical degrees. If they were in spatial degrees their width would increase as the angle varied from boresight. Harmonic and nonharmonic implementations are shown. In harmonic implementations the most closely spaced antennas ($\lambda/2$) provide a completely unambiguous output over $\pm 90^\circ$ spatial degrees. This unambiguous output resolves the ambiguities of the other antenna pair whose phase changes by two cycles over the ± 90 spatial degrees. In particular, while cell 7 of the λ output could be interpreted as being in two different spatial areas, the ambiguity is resolved by cell 12 of the $\lambda/2$ output. Additional baseline extensions are treated in the same way.

An error made in resolving interferometer ambiguities is called a

gross error. Immunity to gross errors (phase tolerance) is a function of the antenna spacing ratio and the degree of phase quantization. Table 2 presents the allowable worst case phase tolerance for infinite quantization for several spacing ratios. For a ratio of 2:1, the closest channel, channel 1, can mistrack the reference channel by $+60^\circ$. While channel 2 can mistrack the reference by -60° before a gross error is made. Uncalibrated systems using antenna ratios of up to 4:1 have been developed, but noise and component mistrack errors require receiver calibration and pulse averaging if spacing ratios larger than 4:1 are desired.

The numbers in the table are phase tolerances only in the sense that if no phase errors exceed that bound, then it is certain that no gross errors will occur. The actual situation is somewhat more complicated. At a given frequency and direction of arrival, the channel phase mistrack acts as a fixed bias, while the noise component produces a variable phase error that has a Gaussian distribution whose variance is inversely proportional to the signal to noise ratio. When the sum of the bias and noise component exceeds the tolerance, a gross error may result. Therefore, the gross error rate is a statistical quantity which depends on the relative proportions of bias and noise in the phase errors, as well as on the total error. Gross error rates of less than 1% are readily achieved. Furthermore, by using pulse to pulse correlation techniques to digitally

ANTENNA SPACING RATIO	WORST CASE PHASE TOLERANCE (DEG)
2:1	60
4:1	36
8:1	20
16:1	10.6

Table 2. Harmonic Interferometer Worst Case Phase Assuming Infinite Quantization.

filter out ambiguities, even higher error rates (lower signal to noise ratios) can be accommodated in a way that is transparent to the ESM processing system.

The nonharmonic interferometer is also shown in Figure 7. In this system no pair of antennas individually provides a completely unambiguous readout over the field of view. Instead, the spacing ratios are chosen in such a way that the ambiguities of each array are separated. A simple truth table interprets the outputs of the two arrays to produce the unambiguous results. The challenge of the interferometer design is to select the antenna spacing ratios in such a way that channel mistrack and noise induced phase errors which cause the phase code to shift will not result in an unacceptable number of gross errors. If phase mistrack is within the specified tolerance, simple logic can

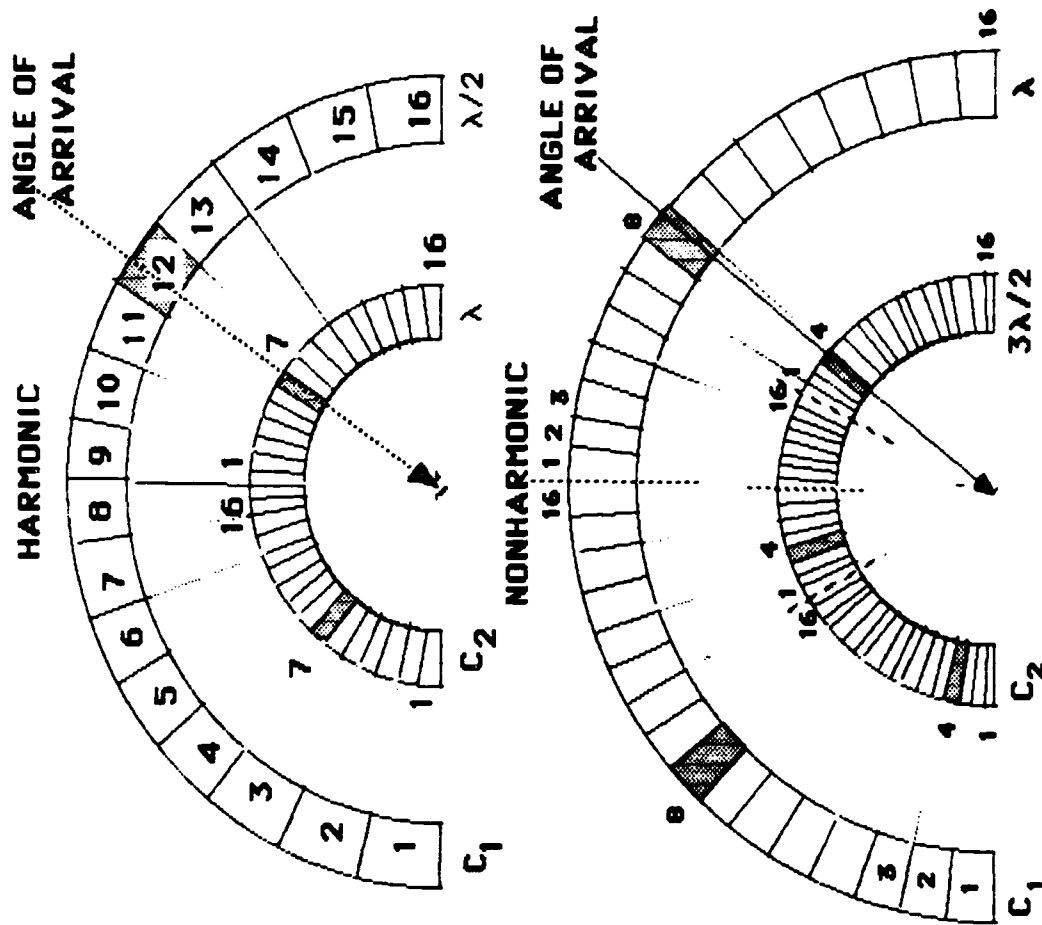
compensate for the antenna/receiver RF and IF phase mistrack. Therefore, simply manipulating a digital code selects the appropriate wide baseline cell. The accuracy of the interferometer system is thus dependent on the phase error that occurs in the widest baseline antenna pair. Non harmonic interferometers built for the military have worked 6 to 1 and 9 to 1 bandwidths and have achieved operational accuracies of 0.1 to 1.0 degree rms. The principal advantage of the nonharmonic interferometer over the harmonic is its greatly increased bandwidth. This is shown in Figure 8, which depicts three spiral antennas on a ground plane. For a harmonic array, as the frequency moves upward, $\lambda/2$ decreases and the closest spaced antennas must move even closer. Eventually the antennas just touch and the element diameter, D , equals $\lambda_{\min}/2$. This design constraint defines the maximum operating fre-

quency. The lowest operating frequency is constrained by the design equation that requires that the antenna perimeter, πD , should equal one wavelength at the lowest frequency of operation for nondegraded antenna gain performance. These two relationships determine the operating bandwidth of the harmonic interferometer array, $f_{\max}/f_{\min} = \pi/2$. Operation even over an octave band results in a significant loss of sensitivity at the lowest frequency. Some wider bandwidth harmonic interferometer systems have been built which do not require the interferometer to work unambiguously over the full 180° field of view. These systems compare the amplitudes received by an element in each quadrant array to select the quadrant or half quadrant from which the signal is emanating. The interferometer need only work unambiguously over the field of view that is reliably selected by the amplitude comparison system. These systems are also presented in Figure 8. The parameter n in this figure is the spacing of the most closely spaced antenna pair, in units of λ_{\min} . When n is equal to 0.707, the interferometer is unambiguous over $\pm 45^\circ$. Similarly, when n is equal to 1.414, the interferometer is unambiguous over $\pm 20.7^\circ$. The bandwidths of these interferometers are 2.22 to 1 and 4.44 to 1, respectively.

The final entry in Figure 8 is a nonharmonic array with n equal to 3. This configuration yields a bandwidth ratio of 9.4 to 1 and an unambiguous field of view of $\pm 90^\circ$. This is far superior to any of the harmonic array designs. Systems of this type

have been built which operate over 2-18 GHz. This system solution depends on very broadband microwave antennas and mixers to reduce the number of antenna/receiver channels from the number required by multiple narrow band system approaches which cover the same bandwidth.

Figure 9 shows the important design parameters of the three element nonharmonic interferometer array and their relationships. As can be seen, d_1 and d_2 have a common factor d_0 . Here, p and q must be integers and must have no common factors. Proper combining of $\Delta\phi_1$ and $\Delta\phi_2$ yields an output that has an unambiguous field of view determined by d_0 . Thus, large antenna elements can be used to provide good low frequency gain, but the array behaves as if the antennas were only spaced d_0 apart rather than pd_0 and qd_0 . The addition of the third antenna not only provides increased accuracy through the increased baseline, but also extends the unambiguous field of view. For a fixed end element spacing, D , the unambiguous field of view of the three element array increases as p and q get larger. At the same time, however, the probability of correct ambiguity resolution decreases. This inverse relationship is one of the tradeoffs that must be made in designing a three element interferometer. Increasing the number of elements increases accuracy, field of view, and gross error performance simultaneously. Thus, the tradeoff is between this improved performance



- TYPICAL RMS ACCURACY - 0.1 TO 1.0°
- UNAMBIGUOUS ARRAY BANDWIDTHS
- 6:1 - AIRBORNE
- 9:1 - SEABORNE

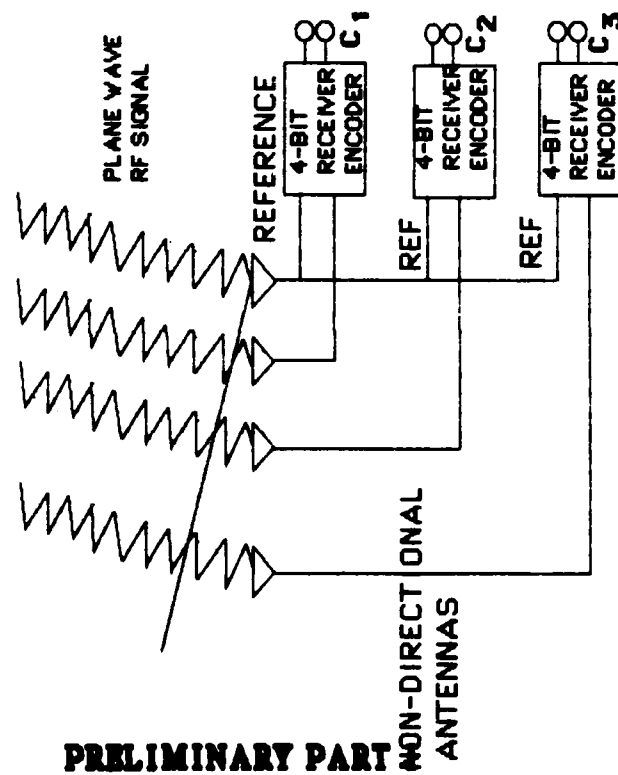
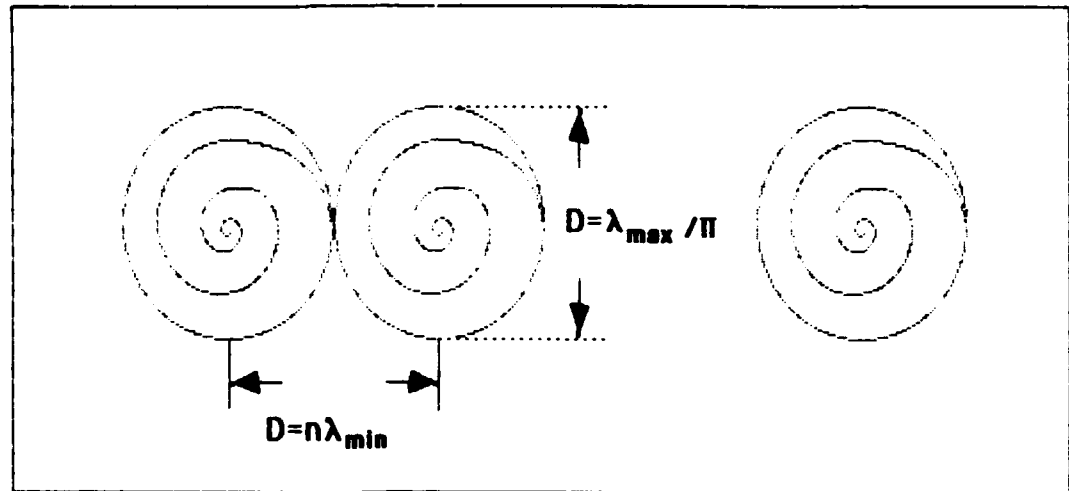


FIGURE 7. MULTIPLE BASELINE INTERFEROMETER



ANTENNA ELEMENT SPACING RATIO	n	BANDWIDTH (F_{\max} / F_{\min})	UNAMBIGUOUS ANGULAR COVERAGE (DEGREES)
HARMONIC	0.5	1.57	± 90
HARMONIC	0.707	2.2	± 45
HARMONIC	1.307	4.1	± 22.5
NONHARMONIC	3.0	9.4	± 90

$$\frac{r_{\max}}{r_{\min}} = n\pi$$

FIGURE 8. INTERFEROMETER BANDWIDTH VS. UNAMBIGUOUS FIELD OF VIEW

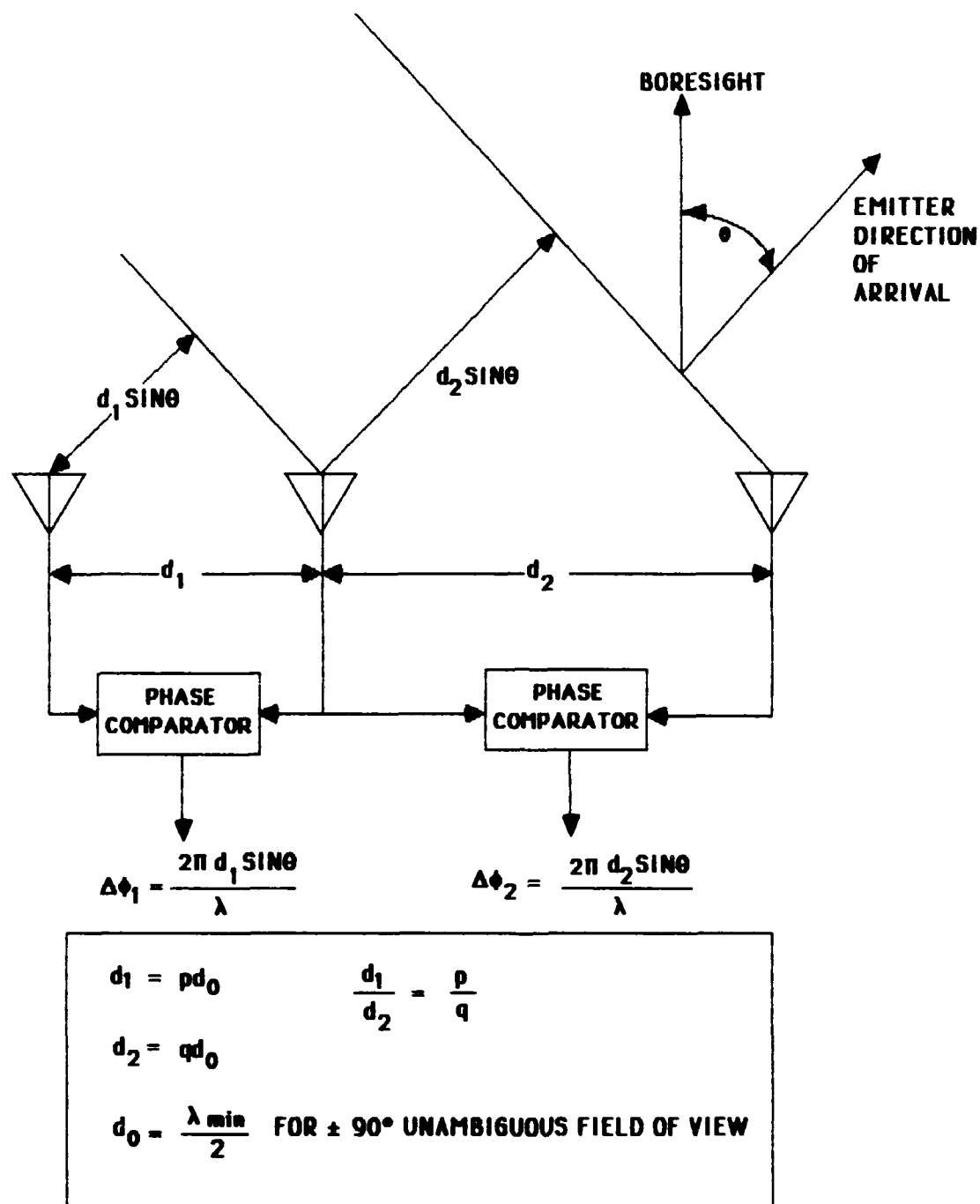


FIGURE 9. 3-ELEMENT INTERFEROMETER

and the greater size, weight, and cost of the total interferometer system.

DF ACCURACY

Interferometer DF accuracy is determined by the measurement accuracy of the widest baseline this measurement error are shown in Figure 10. Accuracy is derived in terms of ω_s , the spacial cell width. The interferometer cell width varies with angle of boresight and frequency. If accuracy information is desired at a given frequency and angle, ω_s is readily calculated and may be substituted into the relationships shown in Figure 10 to derive the accuracy.

The variation of DOA accuracy with frequency and angle of boresight is shown in Figure 11 where DOA accuracy is plotted on polar coordinates. The angle represents the angle off boresight and the radius is the DOA accuracy. For the usual condition where frequency correction introduces a negligible error, the overall error is a straight line on polar coordinates. As can be seen, there is a wide variation in DF accuracy over the frequency range and spatial field of view. If the rms accuracy, which describes expected performance over the entire frequency and angle field of view, is desired, the RMS spatial cell width is determined and substituted into the relationships shown in Figure 10.

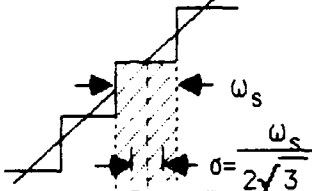
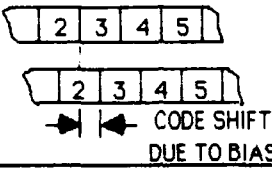
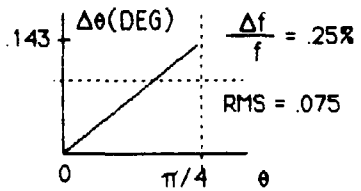
The columns on the right of Figure 10 present the RMS phase error as well as the spatial angular error that results from a system that oper-

ates over a 6:1 frequency range and has a maximum end element separation of 20λ , where λ is the wavelength of the highest operating frequency. The major error components are bias, which includes antenna and receiver channel mistrack, and receiver noise. Typically, multioctave microwave antennas can track to 6 electrical degrees and receivers to 9 electrical degrees. This results in a total RMS phase mistrack of 11 electrical degrees. At a 16 dB signal-to-noise ratio (the threshold level of many modern ESM systems), the RMS phase noise is 9 electrical degrees. The quantization error can be made arbitrarily small, and is selected to be compatible with the other error sources. Frequency must be known so as to properly interpret the spacing, d , in wavelengths. The induced angular error in degrees varies as in equation 8.

$$\Delta\theta = (\Delta f/f) 57.3 \tan\theta \quad (8)$$

Thus, the frequency error does not cause a DF error at boresight ($\theta = 0^\circ$). For a quadrant system, the peak error in degrees is $(\Delta f/f) 57.3$ at 45° . Most modern ESM systems measure frequencies to at least 0.25% RMS which yields a negligible spatial error. For an uncalibrated system, then, the overall phase error for a single pulse measurement is 15.7 electrical degrees. This translates into a RMS spatial accuracy of 0.62° . The receiver noise can be made negligible by pulse averaging. An 8 pulse average reduces the phase noise to 3.2° RMS and yields an overall spatial accuracy

PASSIVE DF: A TUTORIAL

		FREQ RANGE	6:1	
		SPATIAL COVERAGE	90°	
		MAX ANT ELEMENT SPACING	20λ	
TYPE ERROR	EXPRESSION	ILLUSTRATION	ELECTRICAL DEGREES	SPATIAL DEGREES
QUANTIZATION	$\frac{\omega_s}{2\sqrt{3}}$		6.5	0.26
BIAS	$\left(\frac{\Delta\phi}{22.5^\circ}\right) \omega_s$		11.0	0.44
IMPERFECT FREQUENCY CORRECTION	$\frac{\Delta f}{f} 57.3 \tan\theta$			0.075
RECEIVER NOISE	$\frac{57.3 \sqrt{\text{SNR}}}{22.5} \omega_s$	1 pulse	9.1	0.36
		8 pulse	3.2	0.13
TOTAL RMS		1 pulse	15.7	.62
		8 pulse	13.2	.53

ω_s = SPATIAL CELL WIDTH (DEGREES)
 $\Delta\phi$ = PHASE MISTRACK (ELECTRICAL DEGREES)
 22.5° = CELL WIDTH (ELECTRICAL DEGREES)
 FOR 4-BIT QUANTIZATION
 $\text{SNR} = 16 \text{ dB}$
 $\frac{\Delta f}{f} = 0.25\% \text{ RMS}$

FIGURE 10. INTERFEROMETER DF ACCURACY MODEL

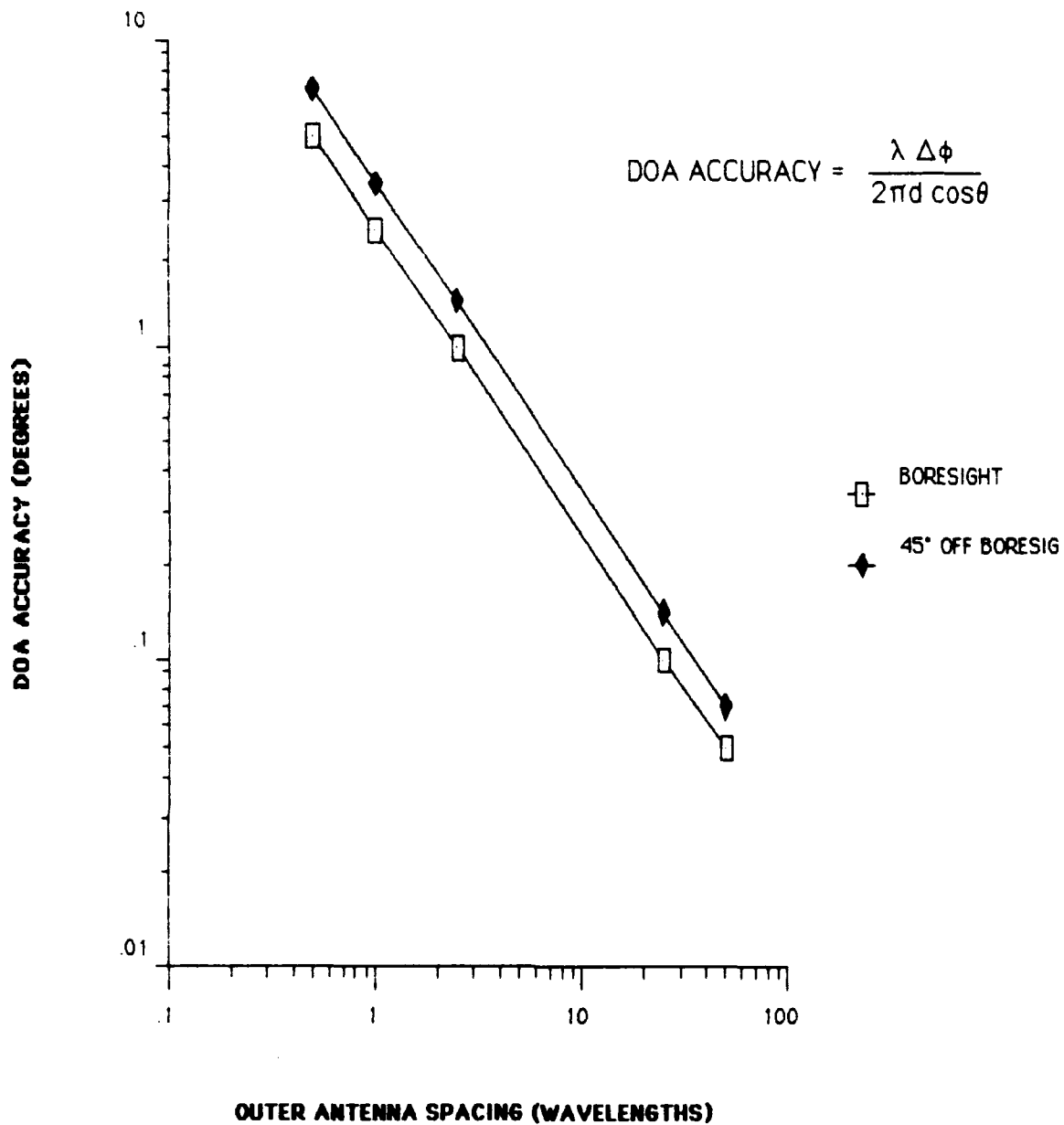


FIGURE 12. DOA ACCURACY AT BORESIGHT AND 45° OFF BORESIGHT AS A FUNCTION OF OUTER ANTENNA SPACING($\Delta\phi=15.7^\circ$)

of 0.53° RMS. If even better performance is desired for $d = 20\lambda$, the receiver mistrack can be removed by calibration. This would reduce the bias error from 11° to 6° , that of the antennas. With an 8 pulse average, the overall phase error is reduced to 9.3° , which yields an overall spatial accuracy of 0.37° RMS.

Figure 12 shows the DF accuracy at boresight and 45° off boresight as a function of outer antenna spacing in wavelengths for an uncalibrated system where the phase mistrack error is 15.7 electrical degrees. This phase mistrack includes both the noise and bias errors shown in Figure 10. This curve yields the end element spacing required to achieve the desired angular accuracy at a given frequency. As the frequency increases for a given d the accuracy improves. Thus, to achieve a 0.1° accuracy a 25λ spacing is required, while a 1° system requires a 2.5λ spacing. If this amount of space is not available then other techniques such as receiver calibration and multiple pulse averaging must be employed.

END

DATE

FILMED
3-88

DTIC